nature neuroscience

Polymodal activation of the endocannabinoid system in the extended amygdala

Nagore Puente[1–6], Yihui Cui[7], Olivier Lassalle[1,2,4–6], Mathieu Lafourcade[1,2], François Georges[1,2], Laurent Venance[7,8], Pedro Grandes[3,8] & Olivier J Manzoni[1,2,4–6,8]

The reason why neurons synthesize more than one endocannabinoid (eCB) and how this is involved in the regulation of synaptic plasticity in a single neuron is not known. We found that 2-arachidonoylglycerol (2-AG) and anandamide mediate different forms of plasticity in the extended amygdala of rats. Dendritic L-type Ca^{2+} channels and the subsequent release of 2-AG acting on presynaptic CB1 receptors triggered retrograde short-term depression. Long-term depression was mediated by postsynaptic mGluR5-dependent release of anandamide acting on postsynaptic TRPV1 receptors. In contrast, 2-AG/CB1R-mediated retrograde signaling mediated both forms of plasticity in the striatum. These data illustrate how the eCB system can function as a polymodal signal integrator to allow the diversification of synaptic plasticity in a single neuron.

The neuronal eCB system is classically described as being composed of three principal signaling lipids (arachidonoylethanolamide, anandamide and 2-AG), the cannabinoid receptor 1 (CB1R), and the proteins responsible for eCBs synthesis, transport and degradation[1–4]. This system modulates synaptic transmission and plasticity in many brain structures, including the bed nucleus of the stria terminalis (BNST), a relay structure of the extended amygdala that integrates stress information into the reward circuitry[5–7]. Activation of CB1R in the BNST filters the cortically driven excitation of dopamine cells *in vivo*[8] and presynaptic CB1Rs inhibit inhibitory and excitatory transmission in BNST slices[9,10], indicating that the eCB system is involved in the integration of stress and reward in this area[8,11].

Recent evidence has suggested that anandamine signaling extends beyond the eCB system and that it acts as an endogenous agonist to transient receptor potential vanilloid type 1 (refs. 10,12–15). Specifically, TRPV1 and anandamide participate in synaptic long-term depression (LTD) in several brain areas[16–19]. The interaction between 2-AG, the mixed vanilloid/cannabinoid anandamide and their receptors, CB1R and TRPV1, is not fully understood. In particular, whether it is anandamide, another fatty acid ethanolamide with TRPV1 bioactivity (such as oleoylethanolamide, OEA)[4,20], and/or 2-AG that controls synaptic plasticity in the BNST is unknown.

We found that different signaling pathways allow a single BNST neuron to engage two distinct forms of synaptic plasticity via the release of either 2-AG or anandamide. 2-AG acted on presynaptic CB1R to mediate retrograde short-term depression (STD), whereas autocrine activation of postsynaptic TRPV1 receptors by anandamide induced LTD.

RESULTS

2-AG and CB1R underlie STD in BNST neurons

In rat BNST slices, the projecting neurons and interneurons can be distinguished on the basis of their electrophysiological properties[21] (**Supplementary Fig. 1**). In both neuronal types, we observed that one can induce depolarization-induced suppression of excitatory postsynaptic currents (EPSCs)[1,2,22], a form of STD, as well as synaptic-driven LTD[1,2,23] (**Supplementary Fig. 1**). Notably, STD and LTD could be induced sequentially in the same BNST neuron without occluding each other and independently of the order at which they were induced (**Fig. 1a**,**b**). AM251, a CB1R antagonist (**Fig. 1c**,**d**), prevented both STD and LTD, suggesting that both forms of plasticity are mediated by the eCB system.

Two core mechanisms of postsynaptic eCB production have been reported: Ca^{2+} entry via voltage-sensitive Ca^{2+} channels (VSCCs) and activation of mGluR1/5 receptors[2–4,22–24]. The L-type Ca^{2+} channels blocker nimodipine abolished STD, suggesting that VSCCs are involved in this form of synaptic plasticity. In contrast, neither MPEP, a specific antagonist of mGluR5 metabotropic glutamate receptors, nor CPCCOEt, an antagonist of mGluR1, inhibited STD (**Fig. 2a,d**).

Elevation of intracellular Ca^{2+} has been shown to enhance phospholipase C activity and contributes to eCB signaling (reviewed in refs. 1,2). We observed that the widely used phospholipase C inhibitor U73122 and the sarcoplasmic/endoplasmic Ca^{2+} pump blocker thapsigargin both prevented STD induction (**Fig. 2d**). Taken together, the data suggest that Ca^{2+} entry through L-type Ca^{2+} channels, phospholipase C activity and intracellular Ca^{2+} stores combine to elevate the intracellular Ca^{2+} concentration to the level that is necessary for STD.

[1]INSERM U862, Physiopathology of Synaptic Plasticity, Neurocentre Magendie, Bordeaux Cedex, France. [2]University of Bordeaux, Bordeaux, France. [3]Department of Neurosciences, Faculty of Medicine and Dentistry, Basque Country University, Leioa, Spain. [4]INSERM U901, Marseille, France. [5]Université de la Méditerranée UMR S901, France. [6]INMED, Marseille, France. [7]UMR CNRS 7241/INSERM U1050, Center of Interdisciplinary Research in Biology, College de France, Paris, France. [8]These authors jointly directed this work. Correspondence should be addressed to L.V. (laurent.venance@college-de-france.fr), P.G. (pedro.grandes@ehu.es) or O.J.M. (olivier.manzoni@inserm.fr).

Received 10 May; accepted 16 August; published online 6 November 2011; doi:10.1038/nn.2974

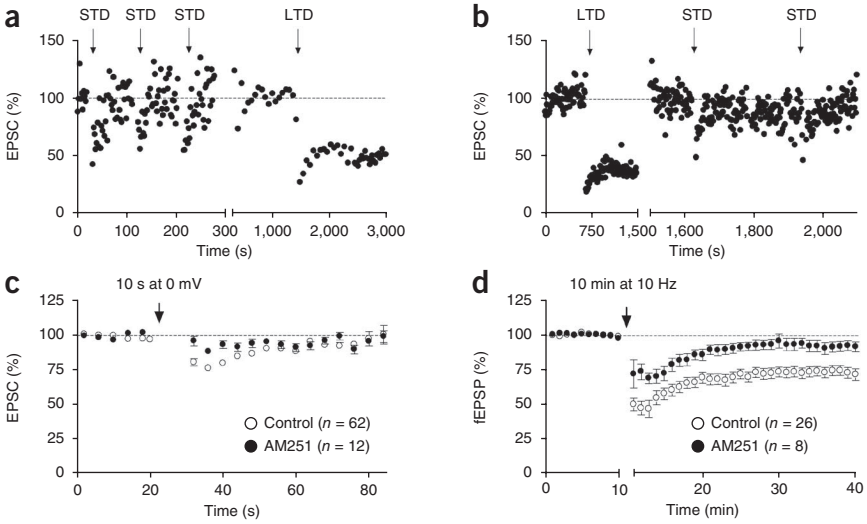

Figure 1 Single BNST neurons express both short-term and long-term eCB-dependent depression. (**a**) After establishing that direct depolarization reproducibly induced STD (postsynaptic cell was depolarized at the time points indicated by the arrows, 0 mV, 10 s), LTD was triggered by synaptic stimulation (10 min, 10 Hz). Note the change of time scale at the axis breaks. (**b**) In another neuron, LTD was triggered first and STD was observed in response to direct depolarization. For representation, each section of the experiment was normalized to its baseline before induction of LTD or STD at the time marked by the axis break. (**c**,**d**) STD and LTD blockade by a CB1R antagonist. Shown are the averages of all the experiments in which STD (**c**) and LTD (**d**) were blocked in slices treated with the CB1R antagonist AM251 (4 μM). $P < 0.05$, Mann Whitney test. Error bars represent s.e.m.

Two lines of evidence suggest that 2-AG is the mediator of STD in the BNST. First, STD was not induced in BNST slices treated with tetrahydrolipstatin (THL)[2,3,25], an inhibitor of the 2-AG–producing enzyme diacylglycerol lipase α (DGL-α; **Fig. 2b**,**d**). Notably, we verified that a second DGL-α inhibitor, RHC-80267 (ref. 26), reproduced the effects of THL (**Fig. 2d**). Second, STD was markedly enhanced in neurons recorded in slices treated with JLZ184 (50 μM), an inhibitor of the 2-AG–inactivating enzyme monoacylglycerol lipase[27] (MGL; **Fig. 2c**,**d**), consistent with the idea that 2-AG underlies STD. We also tested whether URB597, an inhibitor of the anandamide-inactivating enzyme fatty acid amide hydrolase (FAAH), could also enhance STD. URB597 has been shown to increase anandamide levels and counteract 2-AG–mediated retrograde plasticity in the striatum[28]. We found that URB597 had no effect on STD (**Fig. 2c**), excluding the involvement of anandamide in this type of plasticity. Finally, as recent findings have suggested that TRPV1 is involved in eCB signaling[16–19], we examined whether TRPV1 has a role in STD. The TRPV1 antagonist capsazepine (10 μM) had no effect on STD (**Fig. 2d**). From these findings, we conclude that CB1R mediates STD in the BNST following activation of L-type VSCC and the release of 2-AG.

Anandamide and TRPV1 mediate LTD in BNST neurons

We next investigated the mechanisms of LTD and found that they were markedly distinct from those mediating STD. LTD was blocked by MPEP (**Fig. 3a**,**f**), but not by the specific mGluR1 antagonist CPCCOEt, indicating that mGluR5's role in this phenomenon is restricted (**Fig. 3f**). To our surprise, but consistent with recent findings that TRPV1 participates in LTD[16–19], we observed that two antagonists of TRPV1, capsazepine (10 μM) and AMG9810 (3 μM)[17], completely prevented the induction of LTD (**Fig. 3b**,**f**). Furthermore, consistent with the idea that functional TRPV1 is present at BNST excitatory synapses, we also observed that the TRPV1 agonist capsaicin inhibited field excitatory postsynaptic potentials (fEPSPs, 88.02 ± 3.49% of baseline, 20 min after perfusion of 10 μM capsaicin, $n = 9$) and that capsaicin activation of TRPV1 occluded LTD (**Fig. 3c**).

Anandamide and ethanolamide, but not 2-AG, are endogenous ligands of TRPV1 (ref. 13). Accordingly, blocking 2-AG production with THL had no effect on LTD, which argues against 2-AG being involved in LTD (**Fig. 3f**). To test the participation of anandamide in LTD, we used a subthreshold induction protocol that does not trigger LTD unless endocannabinoid hydrolysis is inhibited[25,29].

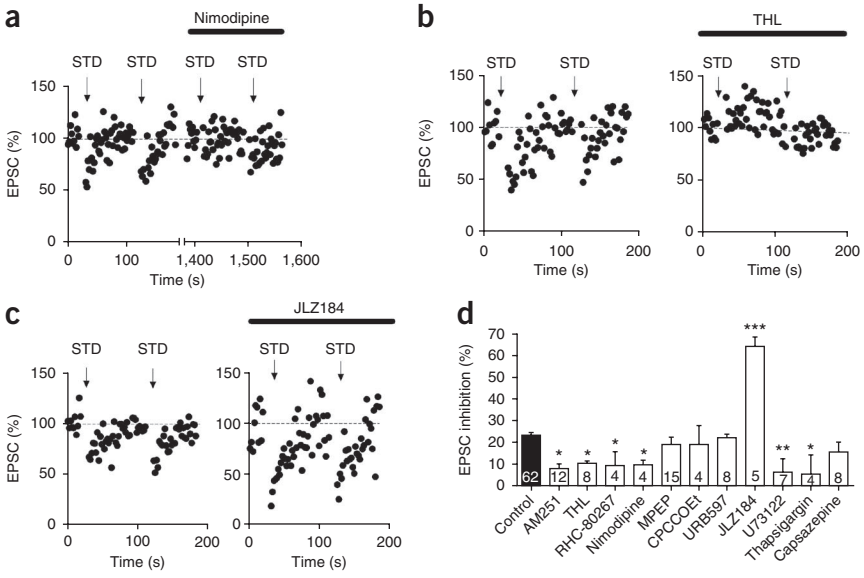

Figure 2 Production of 2-AG mediates STD through L-type Ca^{2+} channels in the BNST. (**a**) STD required L-type Ca^{2+} channels. STD was reliably induced in normal medium and blocked by nimodipine (1 μM). Note the change of time scale at the axis breaks. (**b**) 2-AG mediated STD. A comparison of STD in control slices (left) and interleaved slice pre-incubated with THL (10 μM, 2 h, right) is shown. (**c**) STD was greatly enhanced in interleaved slices where 2-AG degradation was blocked with JLZ184 (50 μM, 2h, 64.1 ± 4.3%, right). (**d**) Summary bar histogram of group experiments. The number indicated in each bar is the number of individual experiments. AM251 (4 μM), THL (10 μM), RHC-80267 (100 μM), nimodipine (1 μM), U73122 (5 μM, >1 h) and thapsigargin (2 μM, >1 h) blocked STD. In contrast, STD was normal in slices incubated with MPEP (10 μM), CPCCOEt (50 μM), capsazepine (10 μM) or URB597 (2 μM). $^*P < 0.05$, $^{**}P < 0.01$, $^{***}P < 0.001$, Mann Whitney test. Error bars represent s.e.m.

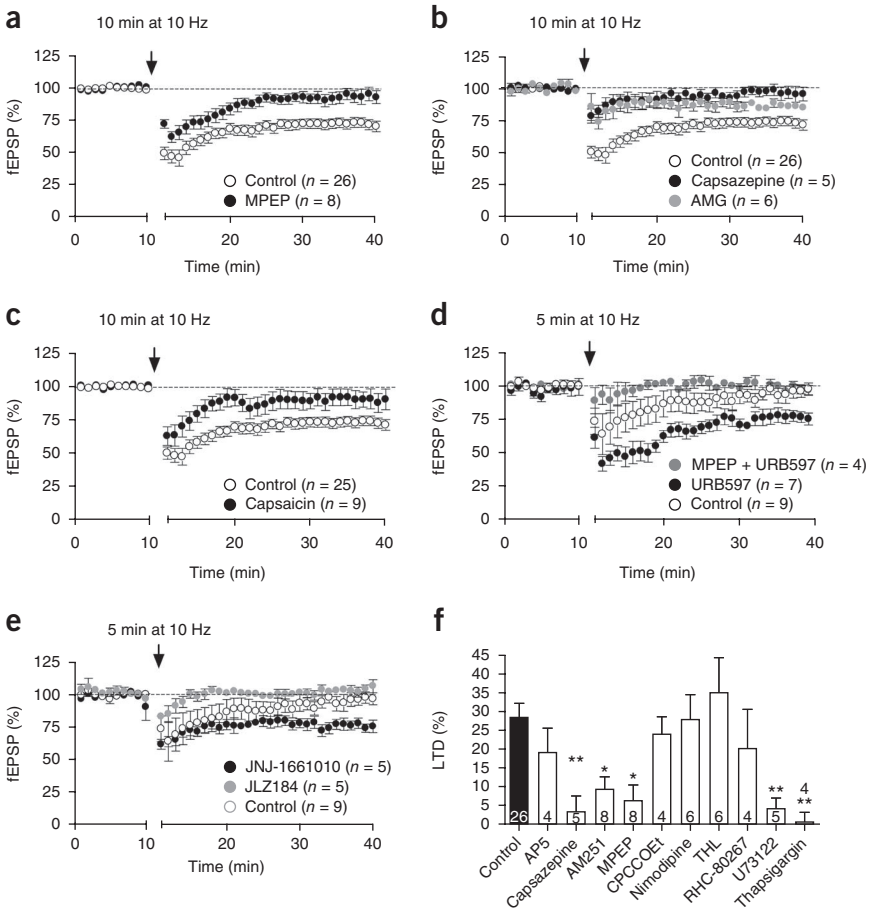

Figure 3 Anandamide and TRPV1 mediates LTD in the BNST. (**a**) mGluR5 inhibition (MPEP, 10 μM, 20 min; black circles) blocked LTD. The 10-min LTD protocol was given during the period indicated by the time break. (**b**) TRPV1 inhibition (capsazepine, 10 μM, black circles; AMG9810, 3 μM, gray circles; both drugs perfused at least 30 min before the LTD protocol) blocked LTD. (**c**) LTD was occluded after perfusion with and in the presence of the TRPV1 agonist capsaicin (10 μM, 8.2 ± 3.4%; black circles), as compared with controls (28.5 ± 4.0%; white circles). (**d**) In control slices, a subthreshold LTD protocol (5 min, 10 Hz) did not elicit LTD (control, 4.7 ± 4.5%; white circles), but it did induce LTD in interleaved slices pre-incubated with URB597 (2 μM, 20 min) to block FAAH and prevent anandamide degradation (23.1 ± 4.5%; black dots). LTD was absent in BNST slices pre-incubated with a cocktail of MPEP and URB597 (5.0 ± 4.3%; gray circles). (**e**) Effects of subthreshold LTD protocol in control conditions (white circles) and in interleaved slices treated with the FAAH inhibitor JNJ-1661010 (1 μM black circles) or with the MGL inhibitor JLZ184 (50 μM, >1 h, gray circles) to prevent the degradation of anandamide or 2-AG, respectively (23.4 ± 3.7% and 0.0 ± 3.4%, respectively). (**f**) Summary bar histogram of all the experiments performed: AM251 (4 μM), capsazepine (10 μM), MPEP (10 μM), U73122 (5 μM, >1 h) and thapsigargin (2 μM, >1 h) blocked LTD, whereas AP5 (50 μM), CPCCOEt (50 μM), nimodipine (1 μM), THL (10 μM) and RHC-80267 (100 μM) had no effect on LTD. $^{*}P < 0.05$, $^{**}P < 0.01$, Mann Whitney test. Error bars represent s.e.m.

We found that a robust LTD was induced in slices treated with URB597 (**Fig. 3d**), but not in slices treated with JLZ184 (**Fig. 3e**). We then performed control experiments to verify that a similar effect was induced with a second FAAH inhibitor[30], JNJ-1661010 (1 μM, **Fig. 3e**). Finally, we made sure that MPEP prevented the induction of LTD by a subthreshold tetanus in the presence of URB597, indicating that mGluR5 is required in this condition (**Fig. 3d**).

In marked contrast with the role of VSCCs in STD, we found that LTD was normal in the presence of nimodipine, which blocks L-type Ca^{2+} channels (**Fig. 3f**). LTD was, however, mediated by mGluR5 (**Fig. 3a**,**f**), which is classically described to be coupled to the phospholipase C signaling pathway and intracellular Ca^{2+} stores[23,31]. Both U73122 and thapsigargin prevented LTD induction (**Fig. 3f**), indicating that phospholipase C activity and intracellular Ca^{2+} stores are involved in LTD in the BNST. Together, these data suggest that LTD in the BNST requires the activation of mGluR5 and the release of anandamide acting at TRPV1.

Localization of synaptic plasticity mediators in the BNST

Our physiological data raise questions about the precise synaptic organization of key proteins underlying both forms of eCB plasticity in the BNST. We recently reported that CB1R is localized in the BNST[9]. We extended these observations and, on the basis of our electrophysiological and pharmacological data, quantified the localization of the mediators of synaptic plasticity, the principal subunit of the neuronal L-type VSCC $Ca_v1.2$, mGluR5, CB1R and TRPV1, using electron microscopy (**Fig. 4**).

Overall, their immunolocalization in the BNST was consistent with their subcellular distribution in other brain structures. Thus, mGluR5 was postsynaptic to asymmetrical synapses made by axon boutons mainly on dendritic spines (**Fig. 4a**), but also on small dendrites (**Fig. 4b**). As expected, mGluR5 was distributed perisynaptically relative to the thick postsynaptic densities of presumptive excitatory synapses (**Fig. 4c**). In contrast, $Ca_v1.2$ (**Fig. 4d**,**e**) was mostly found at extrasynaptic sites beyond the postsynaptic specializations of axon terminal synapses made on somatodendritic membranes (**Fig. 4f**). As we observed previously[9], CB1R labeling occurred at presynaptic terminals making asymmetrical synapses with dendritic spines and small dendrites (**Fig. 4g**,**h**). CB1R immunoparticles were mostly concentrated perisynaptically, but were also found at extrasynaptic sites (**Fig. 4i**). In marked contrast, TRPV1 immunolabeling was enriched in dendritic compartments (**Fig. 4j**,**k**), with a perisynaptic and extrasynaptic distribution (**Fig. 4l**) relative to the thick postsynaptic densities of asymmetrical synapses.

Together, these data indicate a clear segregation of the different proteins that underlie STD and LTD in the BNST. TRPV1 and mGluR5 were enriched in postsynaptic spines and $Ca_v1.2$ was also located on postsynaptic membranes, but further away from active synapses, whereas CB1R was found exclusively presynaptically.

In the striatum, 2-AG and CB1R mediate both STD and LTD

We finally interrogated another brain region with similarities to the BNST. We chose to record from dorsal striatum neurons for two reasons. First, the BNST is a part of the extended amygdala that has a very strong relationship with striato-pallidal networks. Second, BNST neurons have a developmental origin similar to that of striatal neurons[5–7].

Output neurons of the dorsal striatum, the so-called medium-sized spiny neuron, express various types of short and long-term plasticity, and we directly compared cortico-striatal[2] and BNST eCB-mediated

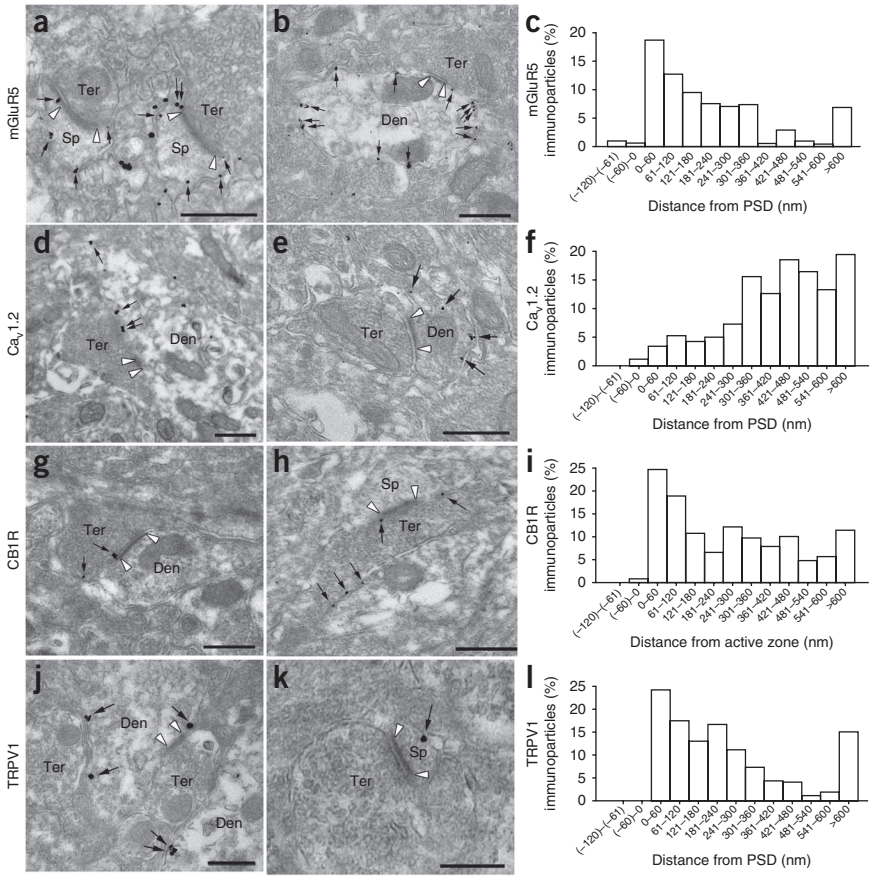

Figure 4 Subcellular and synaptic localization of mGluR5, $Ca_v1.2$, CB1R and TRPV1 in BNST. (**a**,**b**) Typical perisynaptic and extrasynaptic localization of mGluR5 immunoparticles (arrows) relative to the edge of postsynaptic densities (white arrowheads) in spines (sp) and dendrites (den) receiving presynaptic terminals (ter). (**c**) Distribution of mGluR5 immunoparticles relative to the postsynaptic density (PSD). The closest perisynaptic region (0–60-nm bin) contained the highest mGluR5 labeling. The total length of neuronal membrane measured was 143.22 µm. (**d**,**e**) $Ca_v1.2$ immunolabeling (arrows) was present on dendritic membranes away from the edge of postsynaptic specializations (white arrowheads) contacted by presynaptic terminals (ter). (**f**) Data presented as in **c** for $Ca_v1.2$. The closest perisynaptic region (0–60-nm bin) contained the lowest $Ca_v1.2$ labeling. The total length of neuronal membrane measured was 186.1 µm. (**g**,**h**) CB1R immunolabeling (arrows) was present perisynaptically and extrasynaptically in axon terminals forming excitatory asymmetrical synapses (white arrowheads) with small dendrites and dendritic spines. (**i**) Data presented as in **c** for CB1R. CB1R was greatly concentrated perisynaptically at both sides of the presynaptic active zone, but immunolabeling also occurred along the presynaptic bouton membrane. The total length of neuronal membrane measured was 128.6 µm. (**j**,**k**) TRPV1 immunoparticles (arrows) were distributed on membranes of dendritic profiles and postsynaptic spines receiving asymmetrical synaptic contacts (white arrowheads) from axon terminals containing round and clear synaptic vesicles. (**l**) Data presented as in **c** for TRPV1. The closest perisynaptic region (0–60-nm bin) contained the highest TRPV1 labeling. The total length of neuronal membrane measured was 96.24 µm. Scale bars represent 0.5 µm.

plasticity. As observed in BNST neurons, STD and LTD could reliably be induced sequentially in the same medium spiny neuron in cortico-striatal slices (**Fig. 5a**). We found that AM251 precluded the induction of STD and LTD, which remained unaffected by capsazepine treatment (**Fig. 5b**). These data suggest that both STD and LTD rely on CB1R rather than TRPV1 at cortico-striatal synapses. We nonetheless tested for the presence of functional TRPV1 at these synapses. Capsaicin inhibited excitatory postsynaptic currents (EPSCs) in striatal output neurons (10 µM, 80.8 ± 3.9% of baseline, $n = 5$). Thus, although TRPV1 was functionally available, it was not involved in cortico-striatal STD and LTD.

2-AG mediated both cortico-striatal STD and LTD; inhibition of the DGL-α with THL impaired the induction of both STD and LTD (**Fig. 5b**,**c**). Furthermore, STD was blocked in the presence of nimodipine, but was unaffected by MPEP or CPCCOEt. No significant LTD was observed after bath-application of MPEP, whereas robust LTD was induced in the presence of CPCCOEt or nimodipine.

We conclude that, similar to the BNST, STD relies on L-type VSCCs, but not on mGluR1 or mGluR5, and that LTD requires activation of mGluR5, but not mGluR1 or L-type Ca^{2+} channels (**Fig. 5b**,**c**).

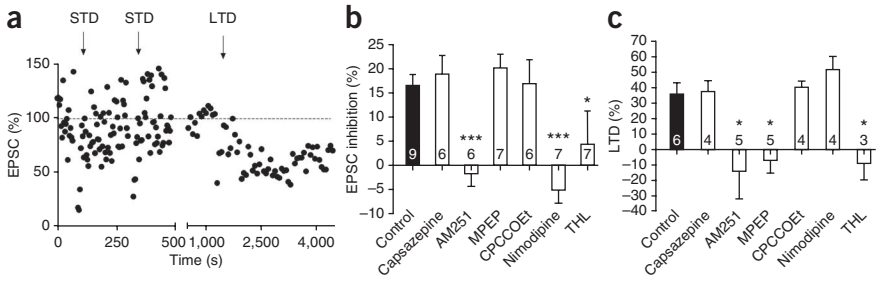

Figure 5 2-AG mediates both STD and LTD in the striatum. (**a**) Single striatum neurons expressed both STD and LTD. Repeated brief depolarizations of a striatum neuron induced STD (the medium spiny neuron was depolarized at the time points indicated by the arrows, 0 mV, 10 s). In the same neuron, LTD was triggered by synaptic stimulation (10 min, 10 Hz). Note the change of time scale at the axis breaks. (**b**) Summary bar histogram of all of the STD experiments. In the striatum, AM251 (4 µM), THL (10 µM, >2 h) and nimodipine (1 µM) blocked STD. The number indicated in each bar is the number of individual experiments. (**c**) Summary bar histogram of all the LTD experiments: AM251 (4 µM), MPEP (10 µM) and THL (10 µM, >2 h) blocked LTD, whereas capsazepine (10 µM) did not affect LTD. $^*P < 0.05$, $^{***}P < 0.001$, Mann Whitney test. Error bars represent s.e.m.

In contrast with the BNST, however, striatal STD and LTD require the release of 2-AG acting on CB1R and are independent of TRPV1.

DISCUSSION

The neuronal eCB system modulates synaptic transmission and plasticity via its two principal signaling lipids anandamide and 2-AG. Initially, studies suggested that both eCB-mediated short- and long-term plasticity were mediated by presynaptic CB1R[1–4]. Recent evidence indicates that anandamine is an endogenous agonist of TRPV1 receptors and is involved in synaptic LTD[10,12–19]. Using electrophysiological and electron microscopy, we examined the interaction between 2-AG, anandamide and their cognate receptors, CB1R and TRPV1, and how this allows a single neuron of the extended amygdala to engage in two distinct forms of synaptic plasticity in response to different stimuli.

First, we found that retrograde somatic depolarization opened L-type VSCCs localized to large dendrites and that the production and release of 2-AG that ensued after DGL-α was activated triggered CB1R-mediated, retrograde, short-lasting inhibition of transmitter release. Second, in the same neuron, activation of mGluR5 receptors and downstream signaling pathways produced anandamide, which activated postsynaptic TRPV1 receptors in an autocrine manner and induced LTD.

The spatio-temporal features of 2-AG and anandamide production, the downstream effectors of TRPV1 and CB1R, and the subsynaptic compartmentalization of the different components of eCB plasticity might help to explain the different kinds of synaptic suppressions observed in the BNST. The timescale of the synaptic suppression correlated with the duration of the stimulus: the brief opening (10 s) of VSCC induced STD, whereas the prolonged activation (10 min) of mGluR5 induced LTD. In addition to the duration of the triggering stimuli, distinct effectors likely mediate CB1R-dependent STD and TRPV1 LTD. Postsynaptic TRPV1 triggers the internalization of postsynaptic AMPA receptors[17,19], a potentially more durable and less labile process than the regulation of presynaptic VSCC and potassium channels by CB1R[1,24,32].

Our data support the idea that the segregation of VSCCs, DGL-α and mGluR5 to different dendritic compartments, combined with the specific postsynaptic and presynaptic localizations of TRPV1 and CB1R, respectively, further define specific synaptic territories expressing STD or LTD. Thus, CB1R-immunopositive axon boutons made excitatory synapses with postsynaptic spines and small dendritic branchlets[9,33,34]. However, the subcellular distribution of the key postsynaptic elements varied depending on the eCB recruited. In the context of eCB LTD, mGluR5 were highly compartmentalized in perisynaptic positions with respect to the postsynaptic density of BNST excitatory synapses, consistent with the distribution of mGluR5 in other brain regions[25,35,36]. In the BNST, DGL-α localized in postsynaptic dendritic and spine compartments away from postsynaptic densities, consistent with the common distribution pattern of DGL-α in somatodendritic domains[33,36–38] (**Supplementary Fig. 2a**,**b**,**f**). The precise subcellular localization of DGL-α, however, is subject to regional variations. For instance, in hippocampal pyramidal neurons, DGL-α is mainly distributed in spine heads and necks[37], but is also found perisynaptic in spine heads[33]. In cerebellar Purkinje neurons, DGL-α is accumulated at the base of spine necks and their surrounding dendritic membranes[37]. Thus, the subcellular DGL-α distribution in BNST neurons is reminiscent of its extrasynaptic localization in the cerebellum. Furthermore, in spite of a seemingly restricted TRPV1 distribution in the brain[39], we found that the perisynaptic annulus of the excitatory postsynaptic densities was enriched in TRPV1 in the BNST, where it coincided with mGluR5 and NAPE-PLD (**Supplementary Fig. 2c–e**,**g**), the chief fatty acid ethanolamide (for example, anandamide, OEA) synthesizing enzyme. Thus, the key proteins underlying eCB-LTD in the BNST are concentrated at the perisynaptic edge of postsynaptic spines and small dendrites receiving excitatory synapses. Taken together, these data demonstrate for the first time, to the best of our knowledge, a co-distribution of mGluR5 and TRPV1 in the perisynaptic signaling machinery[38] that controls the anandamide production involved in eCB LTD at spines and dendritic domains in BNST neurons.

With respect to STD, we found that the principal calcium channel subunit $Ca_v1.2$ was preferentially localized to dendritic sites, well separated from the edge of postsynaptic densities, as has been reported in the hippocampus[40]. Thus, the extrasynaptic dendritic localization of $Ca_v1.2$ matches that of DGL-α in a manner compatible with their putative role in eCB STD in BNST neurons.

Comparing the underpinnings of LTD and STD in the striatum and the BNST revealed marked similarities between two structures of similar developmental origin[5–7]. First, we found that the processes governing STD at cortico-striatal and BNST synapses were identical: opening of VSCC-induced calcium-dependent synthesis of 2-AG, which activates presynaptic CB1R. Second, there were extended similarities in the membrane receptors (mGluR5) and the underlying transduction cascade (intracellular Ca^{2+} stores, phospholipase C) leading to synaptically induced LTD in these structures. The one and only divergence was that anandamide LTD was mediated by TRPV1 in the BNST and by CB1R in the striatum. Although our functional findings confirmed the description of TRPV1 at cortico-striatal synapses[4,41], our results indicate that they were not engaged during the induction of STD or LTD in our experimental conditions. Notably, CB1R are also highly expressed in the striatum[4,41]. In all cases, the physiological patterns that allow the functional recruitment of TRPV1 at cortico-striatal synapses remain unknown. The levels of 2-AG are at least tenfold larger than those of anandamide in striatum[42], a structure in which the activation of group I mGluRs has been shown to trigger the biosynthesis of 2-AG, but not anandamide[43]. Thus, all available data suggest a prominent role of CB1R and 2-AG in eCB-mediated control of striatal excitatory synapses. Anandamide and 2-AG levels vary on diurnal dark and light phases[44], and it is possible that the two eCBs could contributed differently to short- and long-term plasticity depending on the circadian rhythms[44].

We previously reported that direct activation of presynaptic CB1R inhibits inhibitory and excitatory transmission in BNST slices[9] and filters the cortically driven excitation of dopamine cells *in vivo*[8]. By showing how TRPV1 and CB1R differentially control synaptic plasticity in the BNST, the present study substantially extends our knowledge of how lipid neurotransmitters and their receptors could participate to the fine-tuning of excitatory transmission in the extended amygdala and to the synaptic integration of stress and reward signals. As suggested elsewhere, "synaptic plasticity and modulation of excitatory transmission within the BNST may result in alterations in anxiety and reward-related behavior"[11]. Although the behavioral correlates of CB1R-mediated STD and TRPV1-mediated LTD in the BNST are beyond the scope of our study, it is possible that the two receptors exert opposing neuromodulatory and behavioral effects via the two different types of plasticity reported here[45–47]. The data raise the possibility that modulation of anandamide levels and/or of TRPV1 in the BNST may be of therapeutic value in the treatment of stress-related disorders and add to the current interest on FAAH and TRPV1 to develop new anxiolytic drugs[48–50]. In conclusion, our findings illustrate the versatility of the endocanabinoid system and how the architecture of postsynaptic signaling components shapes the signaling mechanisms that cooperate to diversify synaptic plasticity at a central synapse.

METHODS

Methods and any associated references are available in the online version of the paper at http://www.nature.com/natureneuroscience/.

Note: Supplementary information is available on the Nature Neuroscience website.

ACKNOWLEDGMENTS

The authors thank N. Stella, M. Sepers and P. Chavis for critical reading of the manuscript, and R. Martinez for invaluable help in setting up the Manzoni laboratory. Work in the Manzoni laboratory was supported by INSERM, Agence National pour la Recherche Neurosciences (Neurologie et Psychiatrie ANR-06-NEURO-043-01) and Région Aquitaine. N.P. was supported by Basque Country Government Postdoctoral grant BFI05.185 and by a Basque Country University grant for PhD Researcher's Specialization. P.G. was supported by Basque Country Government grant GIC07/70-IT-432-07, by Ministerio de Ciencia e Innovación (SAF2009-07065) and by "Red de Trastornos Adictivos," RETICS, Instituto de Salud Carlos III, MICINN, grant RD07/0001/2001. Y.C. was supported by the Neuroscience School of Paris, Agence National pour la Recherche Neurosciences "Mobil," INSERM and College de France.

AUTHOR CONTRIBUTIONS

N.P. performed the BNST electrophysiology and all of the electron microscopy experiments, conducted the data analyses, and contributed to the design of the experiments. Y.C. performed the striatum electrophysiology experiments and conducted the data analyses. O.L. and M.L. performed part of the BNST electrophysiology and conducted the data analyses. F.G. introduced the BNST preparation to the laboratory. P.G. designed the electron microscopy experiments and wrote the manuscript. L.V. designed the striatal electrophysiology experiments and wrote the manuscript. O.J.M. contributed to the design of all the experiments, supervised the project and wrote the manuscript.

COMPETING FINANCIAL INTERESTS

The authors declare no competing financial interests.

Published online at http://www.nature.com/natureneuroscience/.
Reprints and permissions information is available online at http://www.nature.com/reprints/index.html.

1. Heifets, B.D. & Castillo, P.E. Endocannabinoid signaling and long-term synaptic plasticity. *Annu. Rev. Physiol.* **71**, 283–306 (2009).
2. Kano, M., Ohno-Shosaku, T., Hashimotodani, Y., Uchigashima, M. & Watanabe, M. Endocannabinoid-mediated control of synaptic transmission. *Physiol. Rev.* **89**, 309–380 (2009).
3. Katona, I. & Freund, T.F. Endocannabinoid signaling as a synaptic circuit breaker in neurological disease. *Nat. Med.* **14**, 923–930 (2008).
4. Piomelli, D. The molecular logic of endocannabinoid signalling. *Nat. Rev. Neurosci.* **4**, 873–884 (2003).
5. Herman, J.P. & Cullinan, W.E. Neurocircuitry of stress: central control of the hypothalamo-pituitary-adrenocortical axis. *Trends Neurosci.* **20**, 78–84 (1997).
6. Jalabert, M., Aston-Jones, G., Herzog, E., Manzoni, O. & Georges, F. Role of the bed nucleus of the stria terminalis in the control of ventral tegmental area dopamine neurons. *Prog. Neuropsychopharmacol. Biol. Psychiatry* **33**, 1336–1346 (2009).
7. Koob, G.F. A role for brain stress systems in addiction. *Neuron* **59**, 11–34 (2008).
8. Massi, L. *et al.* Cannabinoid receptors in the bed nucleus of the stria terminalis control cortical excitation of midbrain dopamine cells *in vivo*. *J. Neurosci.* **28**, 10496–10508 (2008).
9. Puente, N. *et al.* Localization and function of the cannabinoid CB1 receptor in the anterolateral bed nucleus of the stria terminalis. *PLoS ONE* **5**, e8869 (2010).
10. Di Marzo, V., Gobbi, G. & Szallasi, A. Brain TRPV1: a depressing TR(i)P down memory lane? *Trends Pharmacol. Sci.* **29**, 594–600 (2008).
11. McElligott, Z.A. & Winder, D.G. Modulation of glutamatergic synaptic transmission in the bed nucleus of the stria terminalis. *Prog. Neuropsychopharmacol. Biol. Psychiatry* **33**, 1329–1335 (2009).
12. Di Marzo, V., Bisogno, T. & De Petrocellis, L. Anandamide: some like it hot. *Trends Pharmacol. Sci.* **22**, 346–349 (2001).
13. Di Marzo, V., De Petrocellis, L., Fezza, F., Ligresti, A. & Bisogno, T. Anandamide receptors. *Prostaglandins Leukot. Essent. Fatty Acids* **66**, 377–391 (2002).
14. Kauer, J.A. & Gibson, H.E. Hot flash: TRPV channels in the brain. *Trends Neurosci.* **32**, 215–224 (2009).
15. Ross, R.A. Anandamide and vanilloid TRPV1 receptors. *Br. J. Pharmacol.* **140**, 790–801 (2003).
16. Maione, S. *et al.* TRPV1 channels control synaptic plasticity in the developing superior colliculus. *J. Physiol. (Lond.)* **587**, 2521–2535 (2009).
17. Chávez, A.E., Chiu, C.Q. & Castillo, P.E. TRPV1 activation by endogenous anandamide triggers postsynaptic long-term depression in dentate gyrus. *Nat. Neurosci.* **13**, 1511–1518 (2011).
18. Gibson, H.E., Edwards, J.G., Page, R.S., Van Hook, M.J. & Kauer, J.A. TRPV1 channels mediate long-term depression at synapses on hippocampal interneurons. *Neuron* **57**, 746–759 (2008).
19. Grueter, B.A., Brasnjo, G. & Malenka, R.C. Postsynaptic TRPV1 triggers cell type–specific long-term depression in the nucleus accumbens. *Nat. Neurosci.* **13**, 1519–1525 (2010).
20. Almási, R. *et al.* Actions of 3-methyl-N-oleoyldopamine, 4-methyl-N-oleoyldopamine and N-oleoylethanolamide on the rat TRPV1 receptor in vitro and in vivo. *Life Sci.* **82**, 644–651 (2008).
21. Dumont, E.C. & Williams, J.T. Noradrenaline triggers $GABA_A$ inhibition of bed nucleus of the stria terminalis neurons projecting to the ventral tegmental area. *J. Neurosci.* **24**, 8198–8204 (2004).
22. Kreitzer, A.C. & Regehr, W.G. Retrograde inhibition of presynaptic calcium influx by endogenous cannabinoids at excitatory synapses onto Purkinje cells. *Neuron* **29**, 717–727 (2001).
23. Robbe, D., Kopf, M., Remaury, A., Bockaert, J. & Manzoni, O.J. Endogenous cannabinoids mediate long-term synaptic depression in the nucleus accumbens. *Proc. Natl. Acad. Sci. USA* **99**, 8384–8388 (2002).
24. Mato, S., Lafourcade, M., Robbe, D., Bakiri, Y. & Manzoni, O.J. Role of the cyclic-AMP/PKA cascade and of P/Q-type Ca^{2+} channels in endocannabinoid-mediated long-term depression in the nucleus accumbens. *Neuropharmacology* **54**, 87–94 (2008).
25. Lafourcade, M. *et al.* Molecular components and functions of the endocannabinoid system in mouse prefrontal cortex. *PLoS ONE* **2**, e709 (2007).
26. Chevaleyre, V. & Castillo, P.E. Heterosynaptic LTD of hippocampal GABAergic synapses: a novel role of endocannabinoids in regulating excitability. *Neuron* **38**, 461–472 (2003).
27. Long, J.Z. *et al.* Selective blockade of 2-arachidonoylglycerol hydrolysis produces cannabinoid behavioral effects. *Nat. Chem. Biol.* **5**, 37–44 (2009).
28. Maccarrone, M. *et al.* Anandamide inhibits metabolism and physiological actions of 2-arachidonoylglycerol in the striatum. *Nat. Neurosci.* **11**, 152–159 (2008).
29. Marrs, W.R. *et al.* The serine hydrolase ABHD6 controls the accumulation and efficacy of 2-AG at cannabinoid receptors. *Nat. Neurosci.* **13**, 951–957 (2010).
30. Karbarz, M.J. *et al.* Biochemical and biological properties of 4-(3-phenyl-[1,2,4] thiadiazol-5-yl)-piperazine-1-carboxylic acid phenylamide, a mechanism-based inhibitor of fatty acid amide hydrolase. *Anesth. Analg.* **108**, 316–329 (2009).
31. Fagni, L., Chavis, P., Ango, F. & Bockaert, J. Complex interactions between mGluRs, intracellular Ca^{2+} stores and ion channels in neurons. *Trends Neurosci.* **23**, 80–88 (2000).
32. Robbe, D., Alonso, G., Duchamp, F., Bockaert, J. & Manzoni, O.J. Localization and mechanisms of action of cannabinoid receptors at the glutamatergic synapses of the mouse nucleus accumbens. *J. Neurosci.* **21**, 109–116 (2001).
33. Katona, I. *et al.* Molecular composition of the endocannabinoid system at glutamatergic synapses. *J. Neurosci.* **26**, 5628–5637 (2006).
34. Kawamura, Y. *et al.* The CB1 cannabinoid receptor is the major cannabinoid receptor at excitatory presynaptic sites in the hippocampus and cerebellum. *J. Neurosci.* **26**, 2991–3001 (2006).
35. Lujan, R., Nusser, Z., Roberts, J.D., Shigemoto, R. & Somogyi, P. Perisynaptic location of metabotropic glutamate receptors mGluR1 and mGluR5 on dendrites and dendritic spines in the rat hippocampus. *Eur. J. Neurosci.* **8**, 1488–1500 (1996).
36. Uchigashima, M. *et al.* Subcellular arrangement of molecules for 2-arachidonoyl-glycerol-mediated retrograde signaling and its physiological contribution to synaptic modulation in the striatum. *J. Neurosci.* **27**, 3663–3676 (2007).
37. Yoshida, T. *et al.* Localization of diacylglycerol lipase-alpha around postsynaptic spine suggests close proximity between production site of an endocannabinoid, 2-arachidonoyl-glycerol, and presynaptic cannabinoid CB1 receptor. *J. Neurosci.* **26**, 4740–4751 (2006).
38. Nyilas, R. *et al.* Molecular architecture of endocannabinoid signaling at nociceptive synapses mediating analgesia. *Eur. J. Neurosci.* **29**, 1964–1978 (2009).
39. Cavanaugh, D.J. *et al.* Trpv1 reporter mice reveal highly restricted brain distribution and functional expression in arteriolar smooth muscle cells. *J. Neurosci.* **31**, 5067–5077 (2011).
40. Tippens, A.L. *et al.* Ultrastructural evidence for pre- and postsynaptic localization of Cav1.2 L-type Ca^{2+} channels in the rat hippocampus. *J. Comp. Neurol.* **506**, 569–583 (2008).
41. Cristino, L. *et al.* Immunohistochemical localization of cannabinoid type 1 and vanilloid transient receptor potential vanilloid type 1 receptors in the mouse brain. *Neuroscience* **139**, 1405–1415 (2006).
42. Bisogno, T. *et al.* Brain regional distribution of endocannabinoids: implications for their biosynthesis and biological function. *Biochem. Biophys. Res. Commun.* **256**, 377–380 (1999).
43. Jung, K.M. *et al.* Stimulation of endocannabinoid formation in brain slice cultures through activation of group I metabotropic glutamate receptors. *Mol. Pharmacol.* **68**, 1196–1202 (2005).
44. Valenti, M. *et al.* Differential diurnal variations of anandamide and 2-arachidonoyl-glycerol levels in rat brain. *Cell. Mol. Life Sci.* **61**, 945–950 (2004).
45. Rubino, T. *et al.* Role in anxiety behavior of the endocannabinoid system in the prefrontal cortex. *Cereb. Cortex* **18**, 1292–1301 (2008).
46. Marsch, R. *et al.* Reduced anxiety, conditioned fear, and hippocampal long-term potentiation in transient receptor potential vanilloid type 1 receptor–deficient mice. *J. Neurosci.* **27**, 832–839 (2007).
47. Starowicz, K. *et al.* Tonic endovanilloid facilitation of glutamate release in brainstem descending antinociceptive pathways. *J. Neurosci.* **27**, 13739–13749 (2007).
48. Gaetani, S. *et al.* The endocannabinoid system as a target for novel anxiolytic and antidepressant drugs. *Int. Rev. Neurobiol.* **85**, 57–72 (2009).
49. Petrosino, S. & Di Marzo, V. FAAH and MAGL inhibitors: therapeutic opportunities from regulating endocannabinoid levels. *Curr. Opin. Investig. Drugs* **11**, 51–62 (2010).
50. Starowicz, K., Cristino, L. & Di Marzo, V. TRPV1 receptors in the central nervous system: potential for previously unforeseen therapeutic applications. *Curr. Pharm. Des.* **14**, 42–54 (2008).

ONLINE METHODS

Electrophysiology. Rats were anesthetized with halothane and decapitated. All animal experiments were performed according to the criteria of the European Communities Council Directive (86/609/EEC) and the US National Institutes of Health *Guide for the Care and Use of Laboratory Animals*.

BNST slices recordings. Whole-cell patch-clamp and extracellular field recordings were made from visualized dorsal BNST cells in rat coronal slices (Sprague-Dawley, 4 weeks old). The brain was sliced (300 µm) in the coronal plane using a vibratome (Integraslice, Campden Instruments) and maintained in physiological saline at 4 °C. Slices containing the BNST were stored at 32–35 °C before being placed in the recording chamber and superfused (2 ml min^{-1}) with artificial cerebrospinal fluid (ACSF) that contained 126 mM NaCl, 2.5 mM KCl, 1.2 mM $MgCl_2$, 2.4 mM $CaCl_2$, 18 mM $NaHCO_3$, 1.2 mM NaH_2PO_4 and 11 mM glucose, and was equilibrated with 95% O_2/5% CO_2. All experiments were carried out at 32–35 °C. The superfusion medium contained picrotoxin (100 µM) to block $GABA_A$ receptors. All drugs were added at the final concentration to the superfusion medium.

To evoke synaptic currents, we delivered stimuli (100–150-µs duration) at 0.1 Hz through a glass electrode filled with ACSF and placed them at the border between the internal capsule and the BNST. The stimulation frequency was 0.5 Hz for the STD experiments.

For extracellular field recordings, the pipette was filled with ACSF. Both the fEPSP area and amplitude were measured. The glutamatergic nature of the extracellular fEPSP was confirmed at the end of each experiment by the application of the non-NMDA ionotropic glutamate receptor antagonist DNQX (20 µM), which completely blocked the synaptic component without altering the nonsynaptic component (data not shown).

For whole-cell patch-clamp experiments, BNST principal neurons were visualized using an upright microscope with infrared illumination. Recordings were made with electrodes containing 128 mM cesium methane-sulfonate (CH_3O_3SCs), 20 mM NaCl, 1 mM $MgCl_2$, 1 mM EGTA, 0.3 mM $CaCl_2$, 2 mM Na^{2+}-ATP, 0.3 mM Na^{+}-GTP, 10 mM glucose, buffered with 10 mM HEPES (pH 7.3), osmolarity 290 mOsm. Electrode resistance was 4–6 MOhms. Neurons were held at −70 mV and both the EPSC area and peak amplitude were measured.

A −2-mV hyperpolarizing pulse was applied before each evoked EPSC to evaluate the access resistance; experiments in which this parameter changed >20% were rejected. Access resistance compensation was not ordinarily used and acceptable access resistance was <25 MOhms. The potential reference of the amplifier was adjusted to zero before breaking into the cell. An Axopatch-1D (Axon Instruments) was used to record the data, which were filtered at 1–2 kHz, digitized at 5 kHz on a DigiData 1200 interface (Axon Instruments) and collected on a PC using Clampex 9.2 (Axon Instruments) and analyzed using Clampfit 9.2 (Axon Instruments).

Striatal slices recordings. Connections between the somatosensory cortex (layer 5) and the dorsal striatum are preserved in a horizontal plane. Patch-clamp recordings were performed in horizontal brain slices (330 µm) prepared with a vibrating blade microtome (VT1200S, Leica Micosystems). For whole-cell recordings, borosilicate glass pipettes of 4–7 MΩ resistance contained 105 mM potassium gluconate, 30 mM KCl, 10 mM HEPES, 10 mM phosphocreatine, 4 mM ATP-Mg, 0.3 mM GTP-Na, 0.3 mM EGTA (adjusted to pH 7.35 with KOH). The composition of the extracellular solution was 125 mM NaCl, 2.5 mM KCl, 25 mM glucose, 25 mM NaHCO3, 1.25 mM NaH2PO4, 2 mM $CaCl_2$, 1 mM $MgCl_2$, 10 µM pyruvic acid bubbled with 95% O_2 and 5% CO_2. All recordings were performed at 34 °C using a temperature control system (bath controller, Luigs & Neumann) and slices were continuously superfused at 2–3 ml min^{-1} with the extracellular solution. Individual neurons were identified using infrared differential interference contrast microscopy with CCD camera (Hamamatsu C2400-07). Signals were amplified using an EPC10-3 amplifier (HEKA Elektronik). Current-clamp recordings were filtered at 2.5 kHz and sampled at 5 kHz and voltage-clamp recordings were filtered at 5 kHz and sampled at 10 kHz using the program Patchmaster v2x32 (HEKA Elektronik). The series resistance was compensated at 75–80%.

Electrical stimulations of the cerebral cortex were performed with a bipolar electrode (Phymep) placed in the layer 5 of the somatosensory cortex. Electrical stimulations were monophasic at constant current (Stimulator WPI or ISO-Flex stimulator controlled by a Master-8, A.M.P.I.). Currents were adjusted to evoke striatal EPSCs ranging in amplitude from 50 to 200 pA. Repetitive control stimuli were applied at 0.1 Hz, a frequency for which neither short- nor long-term synaptic efficacy changes in EPSC amplitudes were induced. Series resistance was monitored and calculated from the response to a hyperpolarizing potential (−5 mV) step during each sweep throughout the experiments and a variation above 20% led to the rejection of the experiment. Repetitive control stimuli were applied at a frequency of 0.1 Hz for 60 min. Drugs were applied in the bath, after recording 10 min of baseline and 10 min before cellular conditioning protocol, and were present continuously until the end of the recording. Off-line analysis was performed using Igor-Pro 6.0.3 (Wavemetrics).

Electron microscopy. Rats (n = 3, Sprague-Dawley, 4 weeks old) were deeply anesthetized with chloral hydrate (400 mg per kg of body weight). All animals were transcardially perfused with phosphate-buffered solution (PBS, 0.1 M, pH 7.4) and then fixed by 500 ml of 0.1% glutaraldehyde, 4% formaldehyde (freshly depolymerized from paraformaldehyde) and 0.2% picric acid in 0.1 M PBS (pH 7.4) prepared at 4 °C. Tissue blocks were extensively rinsed in 0.1 M PBS (pH 7.4). Rostral vibrosections containing the BNST were cut at 50 µm and collected in 0.1M PB (pH 7.4) at 22 ± 2 °C. Sections were pre-incubated in a blocking solution of 10% bovine serum albumin (BSA), 0.1% sodium azide and 0.02% saponin (vol/vol) prepared in Tris-HCl buffered saline (TBS, pH 7.4) for 30 min at 22 ± 2 °C.

A pre-embedding silver-intensified immunogold method was used for the localization of mGluR5, $Ca_v1.2$, CB1R, TRPV1, DGL-α and NAPE-PLD proteins. For primary polyclonal antibodies, we used guinea pig antibody to mGluR5 (2 µg ml^{-1}, mGluR5-GP-Af270-1, Frontier Science), rabbit antibody to $Ca_v1.2$ (4 µg ml^{-1}, α1c, Alomone Labs), goat antibody to CB1 (2 µg ml^{-1}, CB1-Go-Af450-1, Frontier Science), goat antibody to TRPV1 (1:100, VR1 (P-19), sc-1249, Santa Cruz Biotechnology), goat antibody to DGL-α (2 µg ml^{-1}, DGLα-Go-Af1080-1, Frontier Science) and guinea pig antibody to NAPE-PLD (4 µg ml^{-1}, NAPE-PLD-GP-Af720-1, Frontier Science). BNST sections were incubated with the primary antibodies in 10% BSA/TBS containing 0.1% sodium azide and 0.004% saponin on a shaker for 1 d at 22 ± 2 °C.

After several washes in 1% BSA/TBS, tissue sections were incubated with secondary antibodies, 1.4-nm gold-labeled rabbit antibody to goat IgG, goat antibody to guinea pig IgG and goat antibody to rabbit IgG (Fab′ fragment, 1:100, Nanoprobes), depending on the primary antibodies, in 1% BSA/TBS with 0.004% saponin on a shaker for 4 h at 22 ± 2 °C. Thereafter, the tissue was washed in 1% BSA/TBS overnight at 4 °C and postfixed in 1% glutaraldehyde in TBS for 10 min at 22 ± 2 °C. Following washes in double-distilled water, gold particles were silver-intensified with a HQ Silver kit (Nanoprobes) for about 12 min in the dark and then washed in 0.1× PBS (pH 7.4). Stained sections were osmicated (1% OsO4 (vol/vol) in 0.1× PBS, pH 7.4, 20 min), dehydrated in graded alcohols to propylene oxide and plastic-embedded flat in Epon 812. We collected 80-nm ultrathin sections on mesh nickel grids, stained with uranyl acetate and lead citrate, and examined them in a Philips EM2008S electron microscope. Tissue preparations were photographed by using a digital camera coupled to the electron microscope.

Semi-quantitative analysis. We obtained 50-µm-thick BNST sections from three rats showing good and reproducible silver-intensified gold particles and cut them at 80 nm. ImageJ (version 1.36, US National Institutes of Health) was used to measure the membrane length. Electron micrographs (10,000–25,000×) were taken from grids (132 µm side) containing silver-intensified gold particles; all of them showed a similar labeling intensity indicating that selected areas were at the same depth. Furthermore, to avoid false negatives, only ultrathin sections in the first 1.5 µm from the surface of the tissue block were examined. Metal particles on postsynaptic and presynaptic membranes were visualized and counted. Positive labeling was considered if at least one immunogold particle was over postsynaptic or presynaptic membrane or within approximately 30 nm from the membranes.

To establish the precise subcellular distribution of mGluR5, $Ca_v1.2$, TRPV1, and the enzymes DGL-α and NAPE-PLD in postsynaptic profiles in relation to the transmitter release site, we measured the frequency of immunoparticles in 60-nm–wide segments of the postsynaptic membrane of starting at the edge of the synaptic specialization for each case. The edge of postsynaptic density and presynaptic active zone was defined as 0 with the synaptic and peri/extrasynaptic side

doi:10.1038/nn.2974

to the left and right, respectively. We have also measured the subcellular position of CB1R in presynaptic boutons. Given that three samples of each protein analyzed did not differ in particle distribution (Kolmogorov-Smirnov test, $P > 0.19$), the data were pooled. ImageJ was used to measure gold particle's distance counted from the edge of the postsynaptic specialization. Lastly, the values were analyzed and displayed using a statistical software package (GraphPad Prism version 4.0, GraphPad Software).

Data analysis. All values are given as mean ± s.e.m. For field recording and patch-clamp experiments, *n* corresponds to the number of individual cells and slices analyzed, with at least four animals being included in each condition. The magnitudes of STD experiments were measured as percentage of the mean amplitudes of consecutive EPSCs after depolarization (acquired between 2 s and 6 s after the end of the pulse) relative to ten EPSCs before depolarization. The magnitudes of LTD experiments were measured as the percentage of the mean amplitudes of the last 10 min of the 30 min after the end of the tetanus. Statistical significance between groups was tested using the Mann-Whitney U test. All statistical tests were performed with GraphPad PRISM.

Drugs. Picrotoxin, nimodipine and THL were from Sigma. AP5, AM251, DNQX, U73122, thapsigargin, JNJ-1661010, RHC-80267, MPEP, capsazepine, capsaicin, WWL70, JZL184 and CPCCOEt were from Tocris. URB597 was from Cayman (SPI-BIO). All other chemicals were from the highest commercial grade available.